

I

Basic Principles and Theory

1

Phase-Coherent Transport

Thomas Schäpers

1.1

Introduction

From elementary quantum mechanics it is known that electrons possess wave properties in addition to their appearance as a particle. Often, these wave properties are difficult to observe directly, the main reason being that in many cases the electron wavelength is quite small—that is, in metals the wavelength of the electrons at the Fermi energy is only of the order of a few nanometers. Therefore, one possible approach to observing the phenomena related to the wave properties of the electrons is to reduce the sample size to dimensions close to the electron wavelength, as performed in a quantum point contact. Nevertheless, the wave nature of the electrons is sometimes revealed under much more relaxed conditions. An essential prerequisite here is that the coherent wave propagation is maintained over sufficiently long distances, so that interference effects can occur. In most cases this condition is only fulfilled at low temperatures in the Kelvin range, where inelastic scattering is suppressed to a large extent.

In diffusive conductors, one possible way to achieve electron interference is if the diffusive motion allows electrons to propagate coherently in closed loops. This so-called “weak localization effect” can even be observed in macroscopic structures. The electron interference can be significantly modified if spin precession (i.e., due to spin-orbit coupling) comes into play. Well-controlled electron interference can be achieved if the wave propagation is guided by the shape of the conductor, and an excellent example in this respect is the Aharonov–Bohm effect, which is observed in ring-shaped conductors.

This discussion of phase-coherent transport in nanostructures begins by introducing the relevant length scales and the different transport regimes in Section 1.2. Subsequently, in Section 1.3 the Landauer–Büttiker formalism and ballistic transport through a split-gate point contact are discussed. Section 1.4 provides an explanation for the weak localization effect, which leads to an enhanced resistance, whilst in Section 1.5 it is shown that spin precession can result in the reversal of the weak localization effect. Phase-coherent transport in ring-shaped structures is discussed in Sections 1.4 and 1.5, while in Section 1.6 it is shown that the finite number of

scattering centers in very small structures can result in pronounced fluctuations in conductance. Although, within this chapter, transport phenomena in two- and one-dimensional structures are outlined, zero-dimensional structures – namely quantum dots – are discussed in detail in Chapter 2.

1.2

Characteristic Length Scales

Transport in nanoelectronic systems can be classified by relating its size to some specific characteristic length scales [1, 2] which determine how the carriers propagate through the sample. In the following sections, the elastic and inelastic mean free path are introduced, which quantify the degree of elastic and inelastic scattering occurring in the structure, respectively. A length scale, which provides information about loss of the phase memory is termed the phase-coherence length.

1.2.1

Elastic Mean Free Path

The elastic mean free path l_e is a measure of the distance between subsequent elastic scattering events. Such events occur due to the fact that the conductor is not ideal but rather contains irregularities in the lattice, such as impurities or dislocations. The scattering can be considered as *elastic*, which means that the electron energy is conserved. A typical example is the scattering of an electron at a charged impurity. If we assume a stationary scattering center, then effectively no energy is transferred during the scattering event, whereas the direction of the electron momentum can change greatly.

In order to determine the elastic mean free path l_e within the Drude model, one must first calculate the average time between elastic scattering events, τ_e . Its value can be extracted from the electron mobility μ_e , given by

$$\mu_e = \frac{e\tau_e}{m^*} \quad (1.1)$$

The quantities m^* and e are the effective electron mass and the elementary charge, respectively. The electron mobility is a measure of the increase of the drift velocity v_{drift} in a conductor with increasing electric field E : $v_{\text{drift}} = -\mu_e E$. In practice, the electron mobility is determined from the electron concentration n_e and the Drude conductivity σ_0 by

$$\mu_e = \frac{\sigma_0}{en_e} \quad (1.2)$$

Experimentally, the electron concentration n_e is obtained from Hall measurements, while the conductivity σ_0 is deduced from resistance measurements at zero magnetic field.

Effectively, only electrons at the Fermi energy E_F contribute to the electron transport. Therefore, the elastic mean free path l_e is given by the length an electron

with the Fermi velocity v_F propagates until it is elastically scattered after the elastic scattering time τ_e :

$$l_e = \tau_e v_F \quad (1.3)$$

As an example, for a typical two-dimensional (2-D) electron gas in an AlGaAs/GaAs heterostructure (see Section 1.3), low-temperature mobilities of around $10^6 \text{ cm}^2 (\text{Vs})^{-1}$ at $n_e = 3 \times 10^{11} \text{ cm}^{-2}$ are achieved. For a 2-D system the Fermi velocity is given by $v_F = \hbar\sqrt{2\pi n_e}/m^*$. With $m^* = 0.067m_e$ and using Equation 1.3, the length of the elastic mean free path is $9 \mu\text{m}$.

1.2.2

Inelastic Mean Free Path

In addition to the elastic scattering discussed above, electron scattering can also be connected to an energy transfer. A typical example is the effect of lattice vibrations on electron transport. An electron moving within a crystal will be scattered by these lattice vibrations and either lose or gain energy, depending on whether it excites the lattice vibrations or is excited by them. As an energy transfer occurs, these scattering processes are considered to be *inelastic*. Similar to the previous discussion, one can define an inelastic scattering length l_{in} as a measure for the length between inelastic scattering events. Besides electron–phonon scattering, electron–electron scattering is another possible process, where a considerable amount of energy can be exchanged between both scattering partners [3].

1.2.3

Phase-Coherence Length

The phase-coherence length l_ϕ is the relevant length scale, which determines if phase-coherent transport can be observed in nanoelectronic systems [2]. It is a measure of the distance that the electron propagates phase coherently before its phase is randomized. At low temperatures, the phase-coherence length can be larger than the elastic mean free path l_e . Thus, a number of elastic scattering events occur before the phase information is finally lost. During an elastic scattering event (i.e., at an impurity), the phase of an electron is not randomized; it is only shifted by well-defined amount. If the electron propagates along the identical path a second time, the phase accumulation will be exactly the same. This is in strong contrast to inelastic scattering events (e.g., electron–phonon scattering), where the scattering target changes with time. Consequently, the phase shift that the electron would acquire is different each time. However, care must be taken to identify l_ϕ right away with the inelastic mean free path l_{in} , as they are not identical in all cases; that is, spin-flip scattering is considered to be phase-breaking and thus contributing to l_ϕ whilst it may be elastic at the same time. In addition, small-energy-transfer electron–electron scattering, which is due to the fluctuation of the electric field produced by the electrons (Nyquist contribution), can contribute to a large extent to l_ϕ [4]. As mentioned above, at low temperatures a number of elastic scattering events occur

Table 1.1 Comparison of the different transport regimes.

Diffusive	Classical	$\lambda_F, l_e \ll L, l_\phi < l_e$
	Quantum	$\lambda_F, l_e \ll L, l_\phi > l_e$
Ballistic	Classical	$\lambda_F \ll L < l_e, l_\phi$
	Quantum	$\lambda_F \approx L < l_e, l_\phi$

until the phase is broken, implying that the characteristic phase-breaking time τ_ϕ is larger than the elastic scattering time τ_e . Owing to the diffusive motion during the time τ_ϕ , the phase-coherence length l_ϕ must be expressed by

$$l_\phi = \sqrt{D\tau_\phi} \quad (1.4)$$

Here, D is the diffusion constant defined as

$$D = \frac{1}{d} v_F^2 \tau_e \quad (1.5)$$

with d the dimensionality of the system. Typical values for the phase-coherence length of an AlGaAs/GaAs 2-D electron gas below 1 K are of the order of several micrometers [5].

1.2.4

Transport Regimes

By comparing l_e and l_ϕ with the dimension L of the sample and the Fermi wavelength λ_F , different transport regimes can be classified, and these are summarized in Table 1.1. For the case where the elastic mean free path l_e is smaller than the dimensions of the sample, many elastic scattering events occur while the electrons propagate through the structure. The carriers are traveling randomly (*diffusive*) through the crystal, as illustrated in Figure 1.1a. If the phase-coherence

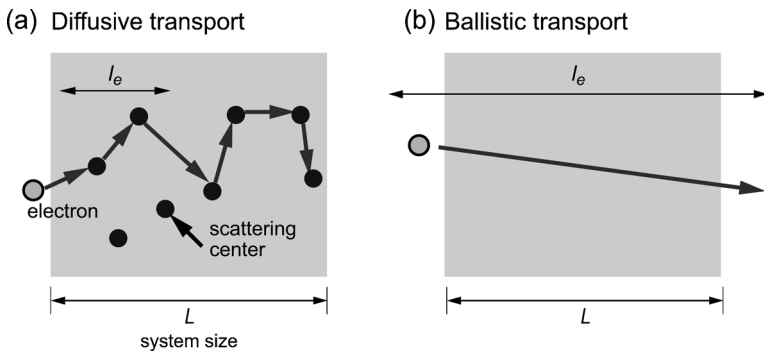


Figure 1.1 Illustration of (a) a diffusive conductor, and (b) a ballistic conductor. In the diffusive transport regime many elastic scattering events occur, while the electron crosses the sample. In the ballistic regime, the electron crosses the sample without any elastic scattering event.

length l_ϕ is shorter than the elastic mean free path l_e , the transport is considered as classical. In contrast, if $l_\phi > l_e$, then quantum effects owing to the wave nature of the electrons can be expected. This diffusive regime is thus called the *quantum* regime. As illustrated in Figure 1.1b, in the case that l_e is larger than the dimensions of the sample, the electrons can transverse the system without any scattering; this regime is called *ballistic*. Depending on the magnitude of the Fermi wavelength λ_F in comparison to the dimension of the sample, the transport can either be regarded as classical ballistic or quantum ballistic. In the following section, ballistic transport will first be discussed, and later the transport phenomena in the diffusive regime.

1.3 Ballistic Transport

In this section transport in the ballistic transport regime will be discussed; that is, where the elastic mean free path exceeds the dimensions of the sample. First, the Landauer–Büttiker formalism is explained, where the resistance of a sample is described in terms of transmission and reflection probabilities, which is a very convenient scheme to analyze the transport in the ballistic regime. Subsequently, the quantized conductance of a split-gate point contact will be discussed, making use of the Landauer–Büttiker formalism.

1.3.1 Landauer–Büttiker Formalism

In order to analyze the electronic transport properties of a sample, usually a current is allowed to flow between two contacts while the response of the system is measured by two voltage probes. The latter are not necessarily different from the current contacts. The ratio between the voltage drop U and the current I can be defined as a *macroscopic resistance*. (The expression *macroscopic* is used here as only the global properties of the sample are measured.)

A very intuitive interpretation of the macroscopic resistance, R , of a sample can be obtained if the so-called Landauer–Büttiker formalism is used [6–9]. In this model, the resistance

$$\mathcal{R}_{mn,kl} = \frac{U_{kl}}{I_{mn}} \quad (1.6)$$

is defined by the voltage measured between contacts k and l and the current flowing between contacts n and m .

In order to keep things simple, the discussion is restricted to a conductor connected via ideal one-dimensional (1-D) ballistic leads to four corresponding reservoirs. The geometry of the sample is depicted in Figure 1.2. The ballistic wires should consist of only a single 1-D. The reservoirs with the corresponding chemical potentials μ_i ($i = 1, \dots, 4$) serve as source and drain for carriers flowing in and out of

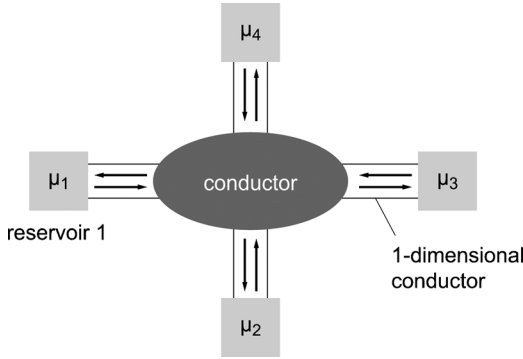


Figure 1.2 Schematic illustration of a four-terminal resistance measurement set-up. The conductor is connected by ideal one-dimensional leads to four corresponding reservoirs.

the conductor. At zero temperature, the i -th reservoir can supply electrons to the conductor up to a maximum energy of μ_i . Each carrier from the lead, which reaches the reservoir is absorbed by the reservoir, irrespective of the phase and energy of the carriers. As discussed above, inelastic scattering is forbidden within the leads, so that electrons once injected into the conductor maintain their energy until they reach one of the reservoirs.

As an example, we will study the current contributions in the 1-D lead 1, which results in the net current I_1 . The current injected from reservoir 1 is given by:

$$I_{inj} = e \int_0^{\mu_1} D_{1D}(E) v(E) dE \quad (1.7)$$

where $v(E)$ is the velocity of the electrons. As the wire is 1-D, the density of states of a 1-D system must be inserted, which is given by

$$D_{1D}(E) = \frac{2}{\hbar v(E)} \quad (1.8)$$

So far, only the states propagating from reservoir 1 are considered, and the density of states used here is half of the commonly known value because there is only one direction of propagation [1]. It can be seen directly that the product of the 1-D density of states $D_{1D}(E)$ and the velocity $v(E)$ is constant, and therefore the current leaving reservoir 1 has the following simple form:

$$I_{inj} = \frac{2e}{\hbar} \mu_1 \quad (1.9)$$

Part of the current supplied by reservoir 1 will be reflected back into the conductor. If R_{ii} is defined as the reflection probability for a reflection of carriers from lead i back into lead i , then the current reflected into lead 1 can be written as

$$I_R = -\frac{2e}{\hbar} R_{ii} \mu_i \quad (1.10)$$

In addition, electrons are transmitted from the other three leads into lead 1. By defining the transmission probability from lead j into lead i ($i \leftarrow j$) as T_{ij} , we arrive at the following expression for the current transmitted into lead 1:

$$I_T = -\frac{2e}{h} \sum_{j=2}^4 T_{1j} \mu_j \quad (1.11)$$

By summing all of these contributions it can be seen that the net current flowing in lead 1 is finally given by:

$$\begin{aligned} I_1 &= I_{inj} + I_R + I_T \\ &= \frac{2e}{h} \left[(1 - R_{11}) \mu_1 - \sum_{j=2}^4 T_{1j} \mu_j \right], \end{aligned} \quad (1.12)$$

or, more generally, the current in lead i is given by

$$I_i = \frac{2e}{h} \left[(1 - R_{ii}) \mu_i - \sum_{j \neq i} T_{ij} \mu_j \right] \quad (1.13)$$

By using Equation 1.13, the above-defined resistance $\mathcal{R}_{mn,kl}$ can be determined for given reflection and transmission probabilities of the sample. According to the initial definition of $\mathcal{R}_{mn,kl}$, as given in Equation 1.6, the net current I_{mn} flows between contacts n and m . The leads k and l do not carry a net current in case of an ideal voltage measurement. The voltage drop U_{kl} is given by the difference of the electrochemical potentials divided by e : $(\mu_k - \mu_l)/e$. In the following section, Equation 1.13 will serve as a basis to describe the transport properties of a split-gate quantum point contact.

1.3.2

Split-Gate Point Contact

In split-gate quantum point contacts the transport is limited to only one dimension. This is obtained by first restricting the propagation of the electrons to a plane. In these so-called “two-dimensional electron gases” (2DEGs), the carriers are confined at an interface of two different semiconductor layers. A typical example of a 2DEG realized in an AlGaAs/GaAs layer system is depicted in Figure 1.3. Here, the carriers are located at the AlGaAs/GaAs interface and, owing to the conduction band offset between AlGaAs and GaAs, a triangular quantum well is formed at the interface. The electrons in the quantum well are supplied by an n -type δ -doped (very thin) layer. In order to prevent ionized impurity scattering, the electrons in the quantum well are separated from the δ -doped layer by an undoped AlGaAs spacer layer. Using this scheme, very large electron mobilities and thus very long elastic mean free paths of the order of several micrometers can be achieved.

A further restriction of the electron propagation to only one dimension can be realized by using split-gate point contacts [10, 11]. As illustrated in Figure 1.4, two opposite gate fingers are separated by a distance of a few hundreds of nanometers. Split-gate electrodes are usually prepared by using electron beam lithography. Since

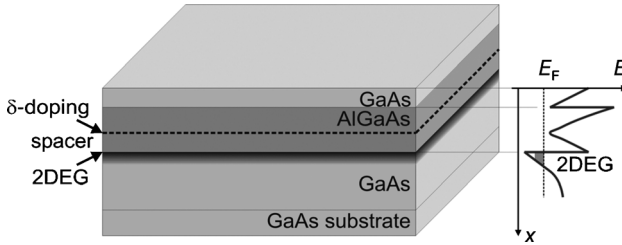


Figure 1.3 Layer sequence of an AlGaAs/GaAs heterostructure containing a two-dimensional electron gas at the AlGaAs/GaAs interface. A schematic illustration of the conduction band profile is shown on the right-hand side.

the Fermi wavelength λ_F of a 2-D electron gas is typically a few tenths of a nanometer, the separation of the split-gates is comparable with λ_F . The length of the channel formed by the gate electrodes is usually smaller than $1 \mu\text{m}$, and thus smaller than the elastic mean free path l_e . According to the classification introduced in Section 1.2, the transport can be considered as ballistic.

By applying a sufficiently large negative voltage to the gate fingers, the underlying 2-D electron gas is depleted underneath the gate fingers (see Figure 1.4a). Only a small opening between the gate fingers remains for the electrons to propagate from one side to the opposite side; however, by varying the gate voltage it is possible to control the effective width of the opening. An increase of the negative bias voltage enlarges the depletion area and thus reduces the opening width. At sufficiently large negative bias voltages the opening can even be closed completely (pinch-off).

Owing to the depletion area underneath the split-gate electrodes, it can be assumed that the electrons in the 2DEG are confined in a potential well along the y -axis, while the free propagation takes place along the x -axis. If the potential profile in the plane of the 2DEG induced by the split-gate electrodes is expressed by $V(x, y)$, the Hamilton

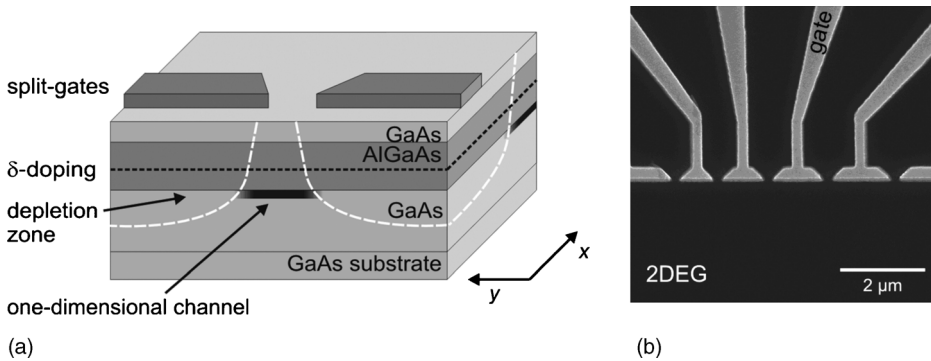


Figure 1.4 (a) Schematic illustration of a split-gate point contact on an AlGaAs/GaAs heterostructures. By applying a negative gate voltage to the split-gate electrodes, the electron gas underneath is depleted. The electrons can only pass the small opening. (b) An electron beam micrograph of split-gate point contacts.

operator has the following form:

$$H = \frac{\hbar^2}{2m^*} \left(\frac{\partial^2}{\partial x^2} + \frac{\partial^2}{\partial y^2} \right) + V(x, y) \quad (1.14)$$

In order to determine the precise shape of the potential $V(x, y)$ as a function of the gate voltage, elaborated self-consistent simulations are required [12]. However, for most applications it is sufficient to assume an approximated potential profile. For low gate voltages an appropriate approximation is a rectangular potential profile, while for higher negative gate voltages the potential well can be approximated by a parabolic potential. As an example, we will consider here the latter potential shape. Due to the short length of the channel formed by the split-gates, the 2-D potential profile will be saddle-shaped. However, if the potential shaped along the constriction is smooth (adiabatic limit), it is sufficient to consider only the narrowest point of the channel, which can be expressed by

$$V(y) = \frac{1}{2} m^* \omega_0^2 y^2 + V_0 \quad (1.15)$$

Here, ω_0 is the characteristic frequency of the parabolic potential, while V_0 represents the height of the inflection point of the saddle-shaped potential. For the energy dispersion of the 1-D subbands in the point contact, we obtain

$$E_n(k_x) = E_n^0 + V_0 + \frac{\hbar^2 k_x^2}{2m^*}, \quad n = 1, 2, 3, \dots, \quad (1.16)$$

with

$$E_n^0 = (n - 1/2)\hbar\omega_0, \quad (1.17)$$

the energy eigenvalues of the harmonic oscillator. By changing the gate voltage at the split-gate electrodes, the effective width of the opening can be adjusted. In the parabolic approximation ω_0 is increased if a more negative gate voltage is applied, and this leads to an increased separation of the energy eigenvalues. As a consequence, lesser levels are occupied up to the Fermi energy (see Figure 1.5a and b).

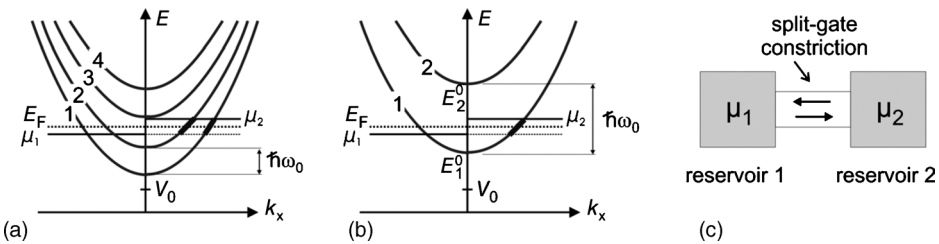


Figure 1.5 (a) Energy dispersion of a one-dimensional channel with the two lowest levels lying below the Fermi energy E_F . (b) Corresponding situation with only one subband occupied. The energy separation between the levels given by $\hbar\omega_0$ is larger

compared to the situation shown in (b). (c) A one-dimensional conductor; that is, the channel formed by the split-gate electrodes, connected by two reservoirs with the electrochemical potential μ_1 and μ_2 , respectively.

Before examining the experimental outcome of measurement of the split-gate point contact resistance, the conduction of a 1-D conductor by using the Landauer–Büttiker formalism will be briefly discussed. It must first be assumed that the conductor is connected on both terminals to reservoirs with the electrochemical potentials μ_1 and μ_2 , respectively (i.e., the 2DEG on both sides of the split-gates), as shown in Figure 1.5c.

For a set-up with only two reservoirs, and where only the lowest subband is occupied, the following expression is obtained according to the Landauer–Büttiker formalism [cf. Equation 1.13]:

$$(h/2e)I = (1 - R_{11})\mu_1 - T_{12}\mu_2 \quad (1.18)$$

$$-(h/2e)I = (1 - R_{22})\mu_2 - T_{21}\mu_1 \quad (1.19)$$

At zero magnetic field ($B = 0$), the transport is time-inversion invariant so that the following relationships hold:

$$T_{12} = T_{21} = T = 1 - R_{11} = 1 - R_{22} \quad (1.20)$$

Thus, finally we arrive at the expression for the conductance of the constriction:

$$G = \frac{I}{U} = \frac{Ie}{\mu_1 - \mu_2} = \frac{2e^2}{h} T \quad (1.21)$$

As illustrated in Figure 1.5b, only carriers with energy between μ_1 and μ_2 contribute to the conductance. If backscattering is neglected ($T = 1$), the conduction through a constriction is simply given by:

$$G = \frac{2e^2}{h}. \quad (1.22)$$

It should be stressed that the constant conductance is a result of the cancellation of the energy dependence of the density of states and the velocity for the 1-D case [cf. Equation 1.7], which is not the case for 2-D or three-dimensional (3-D) systems. In analogy, the conductance can be calculated if N subbands are occupied. The occupied subbands taking part in the transport are usually called channels; the situation for two channels ($N = 2$) is illustrated in Figure 1.5a. If N one-dimensional channels are assumed, then the total transmission probability from reservoir j to reservoir i ($i \leftarrow j$) can be expressed as

$$T_{ij} = \sum_{mn}^N T_{ij,mn} \quad (1.23)$$

where $T_{ij,mn}$ denotes the transmission probability from the n -th subband of lead j into the m -th subband of lead i . If ideal transmission and no intersubband scattering is assumed, then the total transmission probability of a 1-D channel with N subbands is given by $T = N$. Thus, each subband contributes with $2e^2/h$ to the conductance so that the total conductance of a constriction with N subbands occupied is given by

$$G = \frac{2e^2}{h} N \quad (1.24)$$

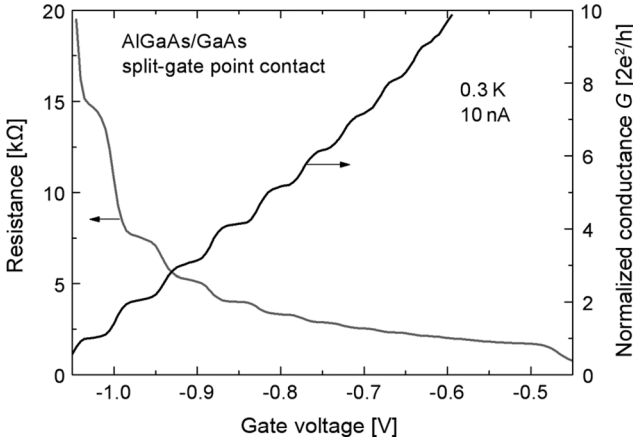


Figure 1.6 Resistance and conductance of an AlGaAs/GaAs split-gate point contact as a function of the gate voltage. The conductance is plotted in units of $2e^2/h$.

This remarkable result indicates that the conductance of a 1-D constriction changes in steps equal to $2e^2/h$, if the number of channels is altered by adjusting the widths of the constriction. The latter can be achieved by applying an appropriate voltage to the split-gate electrodes.

An experimental result of the resistance and conductance of quantum point contact based on a 2DEG in an AlGaAs/GaAs heterostructure is shown in Figure 1.6. With a more negative gate voltage, the resistance of the point contact increases, as the width of the constriction becomes increasingly narrower. As can be seen in Figure 1.6, if the conductance G is plotted, it can clearly be seen that G decreases stepwise by multiples of $2e^2/h$ with increasing negative gate voltage.

The experimentally observed curves can deviate in many aspects from the ideal curves. The calculations given above were restricted to zero temperature, but at finite temperatures the broadening of the Fermi distribution function results in a broadening of the steps owing to the partial occupation and emptying of the 1-D channels. The geometrical shape of the point contact opening also affects the transmission through the point contact. For example, sharp edges of the point contact opening can result in reflections of the incoming and transmitted electrons waves at the inlet and outlet of the 1-D channel. As a result, oscillations are expected in the plateaus of the steps [13, 14].

1.4 Weak Localization

Interference effects of electron waves due to phase coherent transport can be seen even in large samples, where the phase coherence length is much smaller than the dimensions of the sample. This effect, called weak localization, results in an increased resistance compared to the classically expected value [15, 16]. Weak localization is observed if the temperature is sufficiently low so that the phase coherence length l_ϕ is

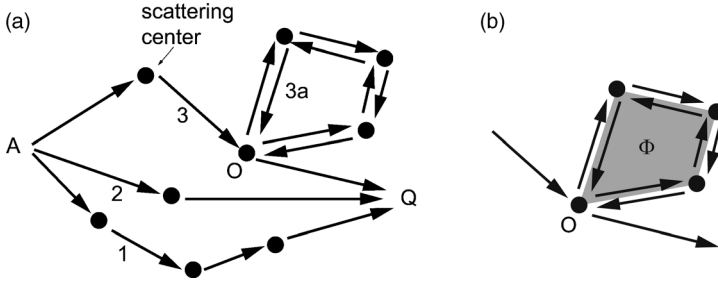


Figure 1.7 (a) Possible trajectories of electrons propagating from point A to Q. The trajectory 3a represents a closed loop. (b) Detail of a closed loop with a magnetic flux Φ penetrating this loop.

larger than the elastic scattering length l_e . As we will see below, the effect of weak localization depends strongly on the dimensionality of the system. The lower the dimension of the system is, the stronger the effect of weak localization is, that is in quasi one-dimensional wire structures weak localization is most pronounced. In order to illustrate the general mechanisms leading to weak localization, we will first introduce a simple model. Later on more quantitative expressions for the conductivity corrections will be given.

1.4.1

Basic Principles

Let us consider a diffusive conductor, in which an electrons starting at point A propagate to point Q. Some typical trajectories of an electron are sketched in Figure 1.7, illustrating that there are many possibilities for an electron to propagate from A to Q.

It is assumed that the elastic mean free path l_e is smaller than the distance between A and Q. Thus, an electron undergoes many elastic scattering events on its way. However, during elastic scattering the electron does not lose its phase memory. If it is assumed that the phase coherence length is longer than the distance between A and Q, the phase information is not lost. By following Feynman, each path j can be described from the initial state A to the final state Q by a complex probability amplitude C_j given by [17, 18]:

$$C_j = c_j \exp(i\varphi_j) \quad (1.25)$$

Here, φ_j is the phase shift that the electron acquires on its way from A to Q while propagating along path j . Often, there are many possible paths for an electron to propagate between A and Q. For example, for free electron propagation the phase accumulation along the path j can be calculated from the action S_j by

$$\varphi_j = \frac{S_j}{\hbar} \quad (1.26)$$

The non-relativistic action S_j is defined by

$$S_j = \int_{t_A}^{t_Q} dt L(\mathbf{r}, \dot{\mathbf{r}}, t) \quad (1.27)$$

with

$$L(\mathbf{r}, \dot{\mathbf{r}}, t) = \frac{m}{2} \dot{\mathbf{r}}^2 \quad (1.28)$$

the Lagrangian function of a free propagating electron. Here, t_A is the time when the electron starts at A , and t_Q the time when it arrives at Q . The quantities \mathbf{r} and $\dot{\mathbf{r}}$ are the position and velocity of the particle, respectively. However, the electron acquires not only a phase shift during free propagation but also well-defined phase shifts by the elastic scattering events, so that the total phase accumulated along the path is the sum of both contributions. The total amplitude for the propagation from A to Q is given by the sum of the amplitudes C_j of all undistinguished paths. Finally, the total probability P_{AQ} for an electron to be transported from A to Q is determined by the square of the total amplitude

$$P_{AQ} = \left| \sum_j c_j e^{i\phi_j} \right|^2 \quad (1.29)$$

In systems with a large number of possible paths, the phases ϕ_j are usually randomly distributed, and therefore the wave nature should have no effect on the electron transport due to averaging. Nevertheless, the fact that an increase of the resistance is observed, compared to the classical transport, is a result of closed loops (see Figure 1.7a, trajectory 3a). Along these loops, an electron can propagate in two opposite orientations with the corresponding complex amplitudes $C_{1,2} = c_{1,2} \exp(i\phi_{1,2})$. The current contribution of the current returning to the starting point of the loop (O) is given by

$$P_{OO} = |C_1 + C_2|^2 = |C_1|^2 + |C_2|^2 + 2\text{Re}(C_1^* C_2) \quad (1.30)$$

Since, for time-reversed paths $c_1 = c_2$ and $\phi_1 = \phi_2$, we obtain

$$|C_1 + C_2|^2 = 4|C_1|^2 \quad (1.31)$$

For classical non-phase-coherent transport, the probability would simply be $|C_1|^2 + |C_2|^2$, which is a factor of 2 smaller than for the phase-coherent case. A larger probability to return to the origin implies that the net current through the sample is reduced. Hence, the carriers are *localized* within the loop. Such localization does not depend on the size of the loop as long as its length is smaller than the phase-coherence length. It is important to note here that constructive interference occurs for *all* possible closed loops in the conductor, and is therefore not averaged out. As a result, the total resistance is increased compared to the classical case.

1.4.2

Weak Localization in One and Two Dimensions

In the following section, it is briefly sketched how a value for the correction of the conductance due to weak localization can be obtained quantitatively [18]. For the weak localization effect we are interested only in those processes where the electrons return to their starting points. The discussion will first be restricted to a 2-D system, for example a 2-D electron gas in an AlGaAs/GaAs heterostructure. A larger number

of scattering centers increase the probability for backscattering of the electrons. The larger the number of scattering centers is, the smaller is the diffusion constant; as a consequence one obtains for the return probability due to diffusive motion: $1/(4\pi Dt)$. For the total return probability, it must be ensured that the phase of the electrons is preserved up to time τ_ϕ , which provides a pre-factor $\exp(-t/\tau_\phi)$. Furthermore, it is required that the electron is at least once elastically scattered; thus, a pre-factor $[1 - \exp(-t/\tau_e)]$ must be included. In total, the correction to the conductance can be expressed as [19, 20]:

$$\begin{aligned}\Delta\sigma_{2D} &= -\frac{2\hbar}{m^*}\sigma_0\int_0^\infty dt\frac{1}{4\pi Dt}(1-e^{-t/\tau_e})e^{-t/\tau_\phi} \\ &= -\frac{e^2}{2\pi^2\hbar}\ln\left(1+\frac{\tau_\phi}{\tau_e}\right)\end{aligned}\quad (1.32)$$

Here, σ_0 is the classical Drude conductivity of a 2-D system. The localization vanishes, if the phase-breaking time τ_ϕ is much smaller than τ_e , since then the logarithmic factor tends towards zero. The ratio of the correction due to weak localization to the Drude conductivity $\Delta\sigma_{2D}/\sigma_0$ is usually small and of the order of $1/k_F l_e$. Here, $k_F = m^* V_F/\hbar$ is the Fermi wavenumber. For a typical 2-D electron gas with $\mu_e = 10^6 \text{ cm}^2 \text{ Vs}^{-1}$ at $n_e = 3 \times 10^{11} \text{ cm}^{-2}$, a correction of less than 0.1% would be expected.

For a quasi 1-D structure of width W with $l_\phi \gg W$, the diffusion is effectively reduced to one dimension, so that the return probability can now be expressed by $W^{-1}(4\pi Dt)^{-1/2}$. The conductivity correction in this case is given by [20]:

$$\Delta\sigma_{1D} = -\frac{e^2}{\pi\hbar}\frac{l_\phi}{W}\left[1 - \left(1 + \frac{\tau_\phi}{\tau_e}\right)^{-1/2}\right]\quad (1.33)$$

A comparison of the 1-D and 2-D cases reveals that the weak localization correction to the conductivity is much larger for the 1-D case. In the latter case, the ratio $\Delta\sigma_{1D}/\sigma_0$ is of the order $(l_\phi/W)(1/k_F l_e)$. If a phase-breaking time of $\tau_\phi = 10^{-10} \text{ s}$ and a width of $W = 200 \text{ nm}$ are assumed, the result is a ratio $\Delta\sigma_{1D}/\sigma_0$ of 6%, for a wire based on the 2-D electron gas as specified above. Clearly, this value is much larger than the corresponding value for a 2-D system.

1.4.3

Weak Localization in a Magnetic Field

If the sample is penetrated by a magnetic field \mathbf{B} , the phase accumulation along a certain trajectory is modified, since the Lagrangian function L [cf. Equation 1.28] of an electron with charge $-e$ contains an additional term

$$L(\mathbf{r}, \dot{\mathbf{r}}, t) = \frac{m}{2}\dot{\mathbf{r}}^2 - e[\dot{\mathbf{r}}\mathbf{A}(\mathbf{r}, t)]\quad (1.34)$$

Here, \mathbf{A} is the vector potential defined by $\mathbf{B} = \text{rot } \mathbf{A}$. In the presence of a vector potential, the probability amplitude C_1 of a closed loop propagated in clockwise

orientation acquires an additional phase factor

$$C_1 \rightarrow C_1 \exp\left(-i \frac{e}{\hbar} \oint A dl\right) = C_1 \exp\left(i \frac{2\pi\Phi}{\Phi_0}\right) \quad (1.35)$$

Here, $\Phi = BS$ is the magnetic flux penetrating the enclosed area S of the loop, with $\Phi_0 = h/e$ the magnetic flux quantum. For the propagation in the opposite orientation one obtains

$$C_2 \rightarrow C_2 \exp\left(-i \frac{2\pi\Phi}{\Phi_0}\right) \quad (1.36)$$

The phase difference accumulated between both time-reversed paths is therefore

$$\Delta\varphi = 4\pi \frac{\Phi}{\Phi_0} \quad (1.37)$$

Thus, if a magnetic field is applied, the property that constructive interference occurs for *all* loops in case of $B = 0$ is lost. Generally, many loops enclosing different areas are found in a diffusive conductor and, depending on the size of the loops, different phase shifts $\Delta\varphi$ develop. Thus, for a particular magnetic field the localization is lifted to a different extent depending on the loop size. If the magnetic field is increased starting from zero, the constructive interference is destroyed first for the largest loops. Finally, if the magnetic field is sufficiently large, the phase difference will be randomly distributed between the ensemble of loops. On average, the degree of localization decreases with increasing magnetic field, resulting in a continuous decrease of the resistance.

For a quantitative approach one must take into account that, in addition to the usual phase breaking at zero magnetic field, the phase is also broken effectively by a magnetic field. Similar to l_φ a length l_m is defined, which is characterized by the condition that the area l_m^2 corresponds to the case that the penetrating flux is equal to Φ_0 . Thus, l_m is defined by $\sqrt{\hbar/eB}$. As outlined above, for a flux Φ_0 the phase difference between time-reversed paths is already significant. The characteristic magnetic relaxation time τ_B related to l_m can be estimated from the relationship $l_m \sim \sqrt{D\tau_B}$, in analogy to Equation 1.4 defining l_φ . The expression that quantitatively describes the increase of the conductivity with increasing magnetic field is given by [21, 22]:

$$\Delta\sigma_{2D}(B) - \Delta\sigma_{2D}(0) = \frac{e^2}{2\pi^2\hbar} \left[\Psi\left(\frac{1}{2} + \frac{\tau_B}{2\tau_\varphi}\right) - \Psi\left(\frac{1}{2} + \frac{\tau_B}{2\tau_e}\right) + \ln\left(\frac{\tau_\varphi}{\tau_e}\right) \right] \quad (1.38)$$

where $\Psi(x)$ is the digamma function. The exact expression for τ_B , which must be inserted into Equation 1.38, is given by $\tau_B = l_m^2/2D$. At zero magnetic fields the relevant maximum size of the loops at which the phase coherence is broken is given by l_φ^2 . In a finite magnetic field, weak localization is suppressed if a noticeable phase shift between time-reversed loops is accumulated. This is the case for loops with the area of about l_m^2 . By comparing both relationships, it is clear that the magnetic field has a significant effect on the conductance for $l_\varphi^2 \approx l_m^2$. This relationship defines a critical

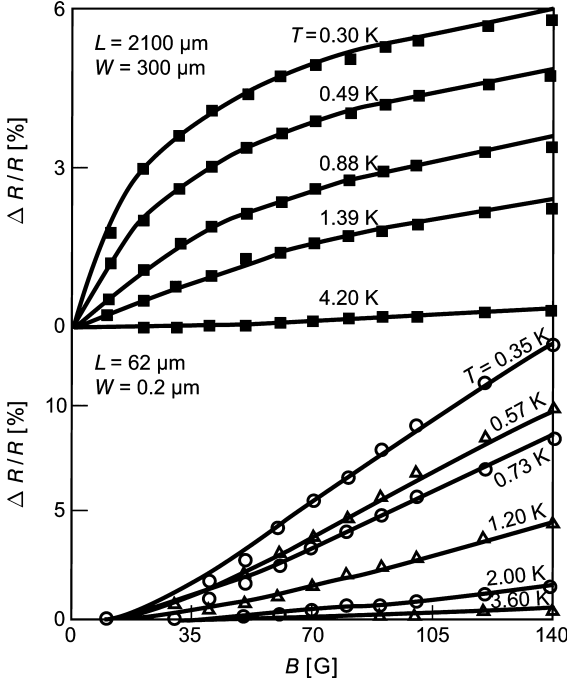


Figure 1.8 Comparison of the weak localization effect in a two-dimensional (upper graph) and a one-dimensional electron gas (lower graph) in AlGaAs/GaAs. For the one-dimensional structures a much higher magnetic field is required to suppress the weak localization effect. (Reprinted with permission from [23]. Copyright (1987) by the American Physical Society.)

magnetic field B_c , which is given by

$$B_c = \frac{\hbar}{2el_\phi^2} \quad (1.39)$$

Thus, at the characteristic field of B_c one expects a suppression of weak localization. For semiconductor structures, l_ϕ may be of the order of $1 \mu\text{m}$, and result in a critical field of about 1 mT . In the case of a 2-D electron gas, weak localization is suppressed at relatively low magnetic fields (see Figure 1.8).

In 1-D systems in the dirty metal limit, defined as $l_e \ll W \ll l_\phi$, the closed trajectories contributing to weak localization are quenched in one direction, with a typical enclosed area of the loop given by $W\sqrt{D\tau_B}$ (see Figure 1.9a). For a unit phase shift this area corresponds to l_m^2 , resulting in a magnetic relaxation time of $\tau_B \sim l_m^4/DW^2$ and a critical field of $B_c \sim \hbar/eWl_\phi$. The full expression for the weak localization correction of one-dimensional systems in the dirty limit is given by [24]

$$\Delta\sigma_{1D}(B) = \frac{e^2}{\pi\hbar} \frac{\sqrt{D}}{W} \left[\left(\frac{1}{\tau_\phi} + \frac{1}{\tau_B} \right)^{-1/2} - \left(\frac{1}{\tau_\phi} + \frac{1}{\tau_e} + \frac{1}{\tau_B} \right)^{-1/2} \right] \quad (1.40)$$

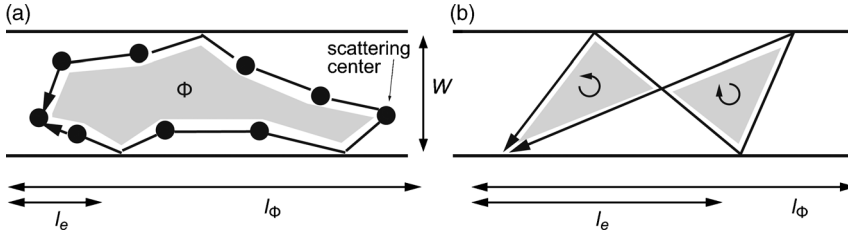


Figure 1.9 (a) Typical closed trajectory in a dirty metal one-dimensional conductor ($l_e \ll W \ll l_\phi$). (b) Typical closed trajectory in a narrow one-dimensional structure with $W \ll l_e$. Here, diffusive boundary scattering results in loops which self-interact. The net flux is cancelled in this configuration.

with magnetic relaxation time in this case given by $\tau_B = 3l_m^4 / WD$. It should be noted that, at zero magnetic fields, Equation 1.32 is recovered. Furthermore, a closer inspection of B_c reveals, that if the width of the wire is reduced, the critical field is increased, ensuring that the weak localization effect is preserved up to much higher magnetic fields compared to the 2-D case. This is confirmed by the measurements shown in Figure 1.8, where the magnetoresistance peak is wider in the 1-D case. In wire structures based on high-mobility, 2-D electron gases, the elastic mean free path l_e may be larger than the width of the wire: $W \ll l_e$. In this ballistic regime, the electrons propagate without any scattering between the wire boundaries. As illustrated in Figure 1.9b, owing to diffusive boundary scattering the typical closed loops will self-interact. As both parts of the loop area are traversed in opposite orientation, the net flux is basically cancelled [20]. Clearly, the flux cancellation results in a further increase of the critical field.

1.5 Spin-Effects: Weak Antilocalization

So far, the effect of spin on the electron interference has been neglected, and this approach is valid as long as the spin orientation is conserved. However, in many materials the spin changes its orientation while the electron propagates along the closed loops, resulting in the weak localization effect.

It can be assumed that $|s\rangle$ is the initial spin state, this generally being a superposition of the spin up $|\uparrow\rangle$ and spin down $|\downarrow\rangle$ states. In principle, there are two possibilities of how the spin orientation can be changed:

- The Elliot–Yafet mechanism. Here, the potential profile of the scattering centers can lead to spin-orbit coupling; this results in a spin rotation, while the electron is scattered at the impurities (see Figure 1.10a).
- The so-called D’yakonov–Perel mechanism, where the spin precesses while the electron propagates *between* the scattering centers (see Figure 1.10b). The origin of the spin precession may either be a lack of inversion symmetry (i.e., in zinc blende

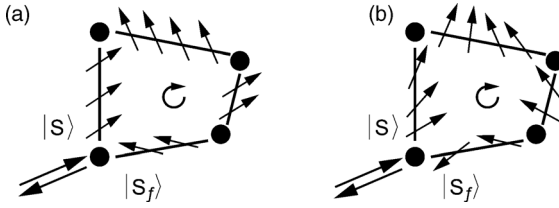


Figure 1.10 (a) Typical closed trajectory in forward direction with spin scattering at the impurities. The initial spin state $|s\rangle$ is transformed to the final spin state $|s_f\rangle$. The spin orientation is preserved while propagation between the scattering centers. (b) The situation where a spin precession occurs while the electron propagates between the scattering centers.

crystals; the Dresselhaus effect [25]), or an asymmetric potential shape of the quantum well forming a 2-D electron gas (the Rashba effect) [26].

Further details on spin precession are provided in Chapter 3 of this volume and Chapter 5 of volume 4 of this series (Bandyopadhyay, S., *Monolithic and Hybrid Spintronics*. In: Schmid, G. (ed), *Nanotechnology*, Vol 4, Chapter 5).

Regardless of the underlying mechanism, if an electron propagates along a closed loop, its spin orientation is changed. The modification of the spin orientation can be expressed by a rotation matrix \mathbf{U} [27]. For the propagation along the loop in forward (f) direction the final state $|s_f\rangle$ can be expressed by

$$|s_f\rangle = \mathbf{U}|s\rangle \quad (1.41)$$

where \mathbf{U} is the corresponding rotation matrix. For propagation along the loop in a backwards directions (b), the final spin state is given by

$$|s_b\rangle = \mathbf{U}^{-1}|s\rangle \quad (1.42)$$

Here, use is made of the fact that the rotation matrix of the counter-clockwise propagation is simply the inverse of \mathbf{U} . For interference between the clockwise and counter-clockwise electron waves, not only the spatial component is relevant but also the interference of the spin component:

$$\begin{aligned} \langle s_b|s_f\rangle &= \langle \mathbf{U}^{-1}s|\mathbf{U}s\rangle \\ &= \langle s|\mathbf{U}^\dagger\mathbf{U}|s\rangle \\ &= \langle s|\mathbf{U}^2|s\rangle. \end{aligned} \quad (1.43)$$

The final expression was obtained by making use of the fact that \mathbf{U} is a unitary matrix: $\mathbf{U}^{-1} = \mathbf{U}^\dagger$, with \mathbf{U}^\dagger the adjoint (complex conjugated and transposed) matrix of \mathbf{U} . Weak localization – and thus constructive interference – is recovered if the spin orientation is conserved in the case that \mathbf{U} is the unit matrix $\mathbf{1}$.

However, if the spin is rotated during electron propagation along a loop, in general no constructive interference can be expected. Moreover, for each loop a different interference will be expected. Interestingly, averaging over all possible trajectories even leads to a reversal of the weak localization effect such that, instead of an increase